Decellularized ovine arteries as small-diameter vascular grafts

Mancuso L[1,2], Gualerzi A[2], Boschetti F[3], Loy F[4] and Cao G[1]

[1] Dipartimento di Ingegneria Meccanica Chimica e dei Materiali, Università degli Studi di Cagliari, Piazza d'Armi, 09123 Cagliari, Italy

[2] BT (Biomedical Tissues) Srl, Viale Monastir km 7,300, 09028 Sestu (CA), Italy

[3] LaBS, Dipartimento di Chimica, Ingegneria Chimica e Materiali "Giulio Natta" Politecnico di Milano Piazza L. da Vinci 32 20133 Milano, Italy

[4] Dipartimento di Scienze Biomediche, Sezione di Citomorfologia, Università degli studi di Cagliari, Cittadella Universitaria di Monserrato, S.S.554 bivio Sestu, 09042, Monserrato (Ca), Italy

E-mail: giacomo.cao@dimcm.unica.it

Received 29 January 2014, revised 26 May 2014
Accepted for publication 12 June 2014
Published 22 July 2014

1. Introduction

Atherosclerosis and its complications still represent the leading cause of death in the developed countries [1]. Such a disease is characterized by the formation of atheromatous plaques that frequently lead to blood vessel occlusion. Medical management of atherosclerosis is focused on the reduction of risk factors involved in the etiology of the disease. However, risk containment is often inadequate and surgical measures are typically required to treat the arterial occlusion caused by atherosclerosis.

Autologous blood vessels represent the best solution for peripheral and coronary bypass. Unfortunately, they are not available in most patients as a result of trauma, vessel diseases, or prior usage [2]. It should be noted that the use of synthetic grafts [3] is satisfactory only for reconstruction of large

arteries (internal diameter > 6 mm). Indeed, synthetic grafts, made of PTFE or Dacron, are not suitable for small diameter arteries (internal diameter < 6 mm), due to severe side effects, such as thrombosis, rejection, intimal hyperplasia, calcification, infection, chronic inflammation, and limited growth potential [4, 5]. These are the main reasons why alternative strategies in vascular surgery of small arteries are urgently needed.

Recently, tissue engineering techniques have been applied to the development of vascular grafts. These strategies involve the use of natural extracellular components, such as collagen or fibrin-based scaffolds seeded with cells [6]. However, their major limitations are represented by the long time needed for the corresponding preparation and the poor mechanical properties obtained [7].

The latest and more attractive engineering approach is based on the use of decellularized extracellular matrix (ECM). Decellularization may be defined as the complete removal of the cellular material from a tissue, through physical, chemical, and enzymatic agents, without adversely affecting the composition, mechanical integrity, and biological activity of the native ECM [8]. Thanks to the decellularization processes recently developed, the host cellular antigens are removed, thus reducing the risk of potential inflammatory response and minimizing immune-mediated tissue rejection [9]. In addition, ECM structure, which is composed of a complex mixture of molecules, is preserved so that adhesion, migration, proliferation, and differentiation of recipient cells may be supported [10]. It should also be noted that the main ECM-proteins of the construct, such as collagen and elastin, are not immunogenic when the vascular graft is implanted [11–15].

Decellularized ECMs have already been used in clinical practice for the successful regeneration of a range of different tissues, including heart valves [16], trachea [17], muscle [18], tendon [19], and abdominal wall [20]. Furthermore, these scaffolds represent a promising solution also for reconstructive surgery for a variety of whole organs, such as heart, lung, liver, and kidney [21].

Decellularized allogenic and xenogenic matrices were also reported to be an attractive option for small-diameter vascular substitutes. Tissues from different locations (small intestine, blood vessels) and species (allogenic, xenogenic donors) and various decellularization protocols have been investigated, thus revealing low immunological response and biomechanical properties comparable to those of native tissues [22].

Along these lines, the aim of this study was to develop an acellular ovine matrix to be used as a suitable scaffold for tissue engineering vascular grafts achievements. The approach comprises the decellularization of ovine carotid arteries following two different protocols. The first one was based on the treatment with SDS only, an ionic detergent used in several studies [23–27] for its capability to solubilize both cytoplasmic and nuclear cellular membranes [28]. The second protocol was based on the combination of a non-ionic detergent (Triton X-100) and an enzymatic treatment (Trypsin). Non ionic detergents have been extensively used in decellularization protocols because of their relatively mild effects upon tissue structure, and among these, Triton X-100 is the most widely adopted [28]. Some studies on Trypsin based tissue decellularization revealed that prolonged enzymatic exposure causes disruption of the ultrastructure and composition of the ECM [28]. Nevertheless, the efficiency of a given decellularization protocol and its effects on ECM structure are greatly dependent upon the tissue and species of interest.

In this study we propose a novel and efficient protocol for ovine carotid decellularization based on the use of detergent and enzymatic treatment, where reagent concentrations and exposure times have been optimized with respect to current literature indications [29, 30]. Cell removal, ECM preservation, biocompatibility, and mechanical properties of the treated vessels compared to native ones are also investigated.

2. Material and methods

2.1. Tissue harvesting

Carotid arteries from adult sheep (*Ovis Aries*) were obtained from a local abattoir (CO.AL.BE. Contu & C.s.n.c., Cagliari). Once they arrived in the laboratory, blood vessels were cleaned from fat and adherent tissue with a scalpel, and samples of approximately 5 cm in length were prepared. Vessels with an internal diameter of 4–5 mm are typically considered. Artery segments were immediately washed for about 30 min at +4 °C in a phosphate buffered saline (PBS) solution containing 1% penicillin/streptomycin, in order to avoid the risk of bacterial contamination. Afterwards vessels were stored at −20 °C before the proposed decellularization processes were applied.

2.2. Decellularization

Decellularization was performed according to two different protocols using a rotating shaker. The first group of blood vessels was immersed in a PBS solution containing 1% sodium dodecyl sulphate (SDS), 1% penicillin/streptomycin, and 2% amphotericin for 36 h. The second one was treated with a PBS solution containing 0.05% Trypsin, 0.02% ethylenediaminetetraacetic acid, 1% penicillin/streptomycin, and 2% amphotericin for 24 hours at 37 °C, and then blood vessels were contacted with an agitated PBS solution containing 1% Triton X-100, 1% penicillin/streptomycin, and 2% amphotericin for 24 more hours. At the end of both treatments, blood vessels were washed with PBS solution for 30 min, and then incubated with 1.2 mg ml^{-1} DNase and RNase in PBS. All reagents were obtained from Sigma-Aldrich (Sigma, St. Louis, MO, USA). In all performed tests, untreated freshly harvested carotids as well as carotids processed similarly to treated ones without detergents and/or enzymes were considered as controls.

2.3. Histology

Immediately after treatments, samples were formalin fixed, dehydrated in an ascending series of alcohols, paraffin

embedded, and cut in 3.5 μm serial sections before performing Hematoxylin and Eosin (H&E) staining. Collagen and elastic fibers were evidenced by taking advantage of Masson's trichrome and Verhoeff-van Gieson staining methods, respectively.

2.4. Vessel thickness measurement

Wall thickness was measured by taking advantage of the image processing software ImageJ (developed by Wayne Rasband, National Institutes of Health, Bethesda, MD; available at http://rsb.info.nih.gov/ij/index.html) and the photomicrographs of H&E stained sections obtained at 10x magnification with Leica DM IL LED equipped with digital camera (Leica Microsystems, Wetzlar, Germany). After proper calibration of the pixel/μm ratio, straight lines orthogonal to the artery luminal surface were manually selected going from the inner to the outer elastic laminae. The ImageJ automatic length calculation allowed a reliable evaluation of the vessel thickness. At least 6 sections per sample were analyzed, with a minimum of 30 measurements per section.

2.5. Immunohistochemistry

Immunohistochemistry was performed on paraffin sections adjacent to those set up for histological analysis. Polyclonal antibodies against collagen type I (Cat.n. NBP1-30054; Novus Biologicals, Cambridge, UK), laminin (Cat.n. NB300-144; Novus Biologicals, Cambridge, UK) and fibronectin (Cat.n. A0245; DakoCytomation, Glostrup, Denmark) were used to establish collagen distribution and the presence of basement membrane proteins. Heat induced antigen retrieval was carried out for collagen and fibronectin immunostaining, whereas trypsin 0.1% in PBS was used for laminin localization. Primary antibodies specific for collagen I and fibronectin were diluted 1:100 and 1:1600, respectively in PBS, and incubated for 1 hour at room temperature. Anti-laminin antibody was diluted 1:500 in PBS and incubated overnight at 4 °C. A goat anti-rabbit immunoglobulin conjugated with alkaline phosphatase (Cat.n. 12–448; EMD Millipore Corporation, Billerica, MA, USA), diluted 1:200 in PBS, allowed primary antibody recognition and immunoreactivity was detected using Fast Red TR/Naphtol AS-MX (Sigma, St. Louis, MO, USA). Sections were counterstained with hematoxylin. Negative controls were obtained by omitting the primary antibody.

2.6. Scanning electron microscopy (SEM)

The carotid arteries either treated or not were immediately prepared for high resolution scanning electron microscopy (HRSEM) observation. Samples were fixed in a mixture of glutaraldehyde 1.25% and paraformaldehyde 1% in cacodylate buffer 0.1 M (pH 7.2) for 2 h at room temperature. After rinsing in a PBS solution, tissues were cut in fragments of 1 mm^3 thickness and treated with 1% osmium tetroxide and $K_3[Fe(CN)_6]$ 1.25% (1:1) for 2 h in darkness as described in the first steps of a variant of the OsO_4 maceration method [31, 32]. Specimens were dehydrated with acetone, subjected to critical point dry, sputtered with platinum (2 nm thickness), and, finally, mounted on an aluminum stub and observed with a Hitachi S4000 FEG HRSEM operated at 15–20 kV.

2.7. DNA quantification

To determine whether the cellular components were completely removed, DNA was extracted from 25 mg of dried decellularized and native carotid samples using a commercially available kit (PureLink Genomic DNA Kits, Invitrogen) and eluted in a final volume of 30 μl, according to the instructions provided. The kit is based on the selective binding of nucleic acids to silica membranes and subsequent elution. Nucleic acids were stored at −20 °C until use. For DNA quantification, the ultraviolet absorbance of the eluted solutions was measured with a spectrophotometer at 260 nm. DNA content is expressed as μg of DNA per mg of sample dry weight.

2.8. Evaluation of human mesenchymal stem cell proliferation in conditioned medium

The influence of residual chemicals introduced by the decellularization protocols was assessed by taking advantage of growth curves related to human mesenchymal stem cells (hMSCs), isolated and characterized as previously described [33]. After the decellularization protocol of ovine carotids was completed, the vessels were incubated in cell culture medium (alpha Minimum Essential Medium, Sigma Aldrich) for 4 days at 4 °C to create conditioned media, as previously described by Mangold [34]. Subsequently, human MSCs at 6^{th} passage were seeded at 4500 cells per well on 96-well plates using either fresh cell culture medium (alpha Minimum Essential Medium supplemented with 20% fetal bovine serum, 1% penicillin/streptomycin and 2 mM L-glutamine, Sigma Aldrich) as control or the conditioned media obtained as described above. After 1, 2, 6, and 7 days of incubation, the cell proliferation was evaluated using the optical densities determined by XTT assay (Cell Proliferation Kit II Roche Diagnostic SpA, Milano, Italy) on the basis of the instructions provided.

2.9. Cell seeding onto decellularized carotids

A fragment of carotids decellularized using SDS or Trypsin and Triton X-100 were cut longitudinal to obtain bidimensional samples of approximately 1.5 cm^2 area under sterile conditions. Samples were then placed with the luminal side up at the bottom of a 24-well plate. Sterile plastic rings were used to make the scaffold adhere to the well. Subsequently, hMSCs at 6^{th} passage were seeded onto the scaffolds at a density of 1×10^4 cells cm^{-2} in culture medium. After 96 h of static culture at 37 °C, cells were fixed in 70% methanol, stained with Giemsa for 5 min, rinsed with PBS, and observed by light microscopy. hMSCs seeded at the same density onto wells without scaffolds served as control of the proliferation. The experiment was performed in triplicate.

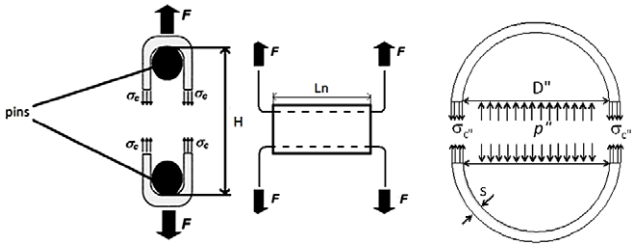

Figure 1. Schematic representation of the ring test. (*h*) is the vertical length between the pin axes (current actuator displacement plus pins spread at zero actuator displacement), L_n is the ring length, (*f*) is the force measured by the machine, σ_c is the circumferential stress acting in the vessel wall.

2.10. Mechanical testing

Samples were subjected to uni-axial and ring tension tests using for both tests an electromagnetic machine (Enduratec Elf 3200, Bose Corporation, Eden Prairie, MN, USA), equipped with a load cell of 220 N. From each original sample, four specimens were obtained: two strips in the longitudinal direction, one strip in the circumferential direction, and one ring, approximately 10 mm long. Longitudinal and circumferential specimens were fixed at the machine grips and elongated under displacement control at a constant rate of 0.1%/s until failure, after 10 preconditioning cycles at the same rate, from 0 to 20% strain. Stress was calculated dividing the machine measured force by the resistant area (thickness times width). Strain was calculated by normalizing the machine actuator displacement with the specimen initial length. Typical stress-strain curves displaying stiffening for increasing strains have been approximated by a bi-linear curve. The low and high strain stiffnesses were therefore obtained by fitting with a straight line the two linear portions of the stress-strain curve, while the relative slope value is assigned to the stiffness.

As schematically represented in figure 1, the obtained rings were mounted on two pins of specially designed grips and subjected to sinusoidal tension tests at 1 Hz and at four different amplitudes, while increasing the initial diameter by 8, 16, 24, and 32%. From the knowledge of the machine displacement $\delta(t)$, the distance between the two pins, h(t) can be evaluated as follows:

$$h(t) = H + \delta(t).$$

The equivalent diameter of the *in vivo* vessel can be calculated by equating the perimeter of the stretched *in vitro* vessel (ring test) to that of the cylindrically shaped vessel (*in vivo*):

$$D_e(t) = (2/\pi)[h(t) + \pi r].$$

where H is the initial distance between pins and r is the pin radius.

The applied force F(t) is related to the wall stress via the equilibrium equation: $F(t) = \sigma_c(t) \times Ln \times 2s$, where Ln is the ring length and s is the specimen thickness. The wall stress σ_c acting *in vivo* in the vessel wall can be evaluated by modeling the vessel as a thin walled cylinder subject to a transmural pressure p(t). Under the hypothesis of uniform pressure distribution within the vessel, the value of σ_c is given by:

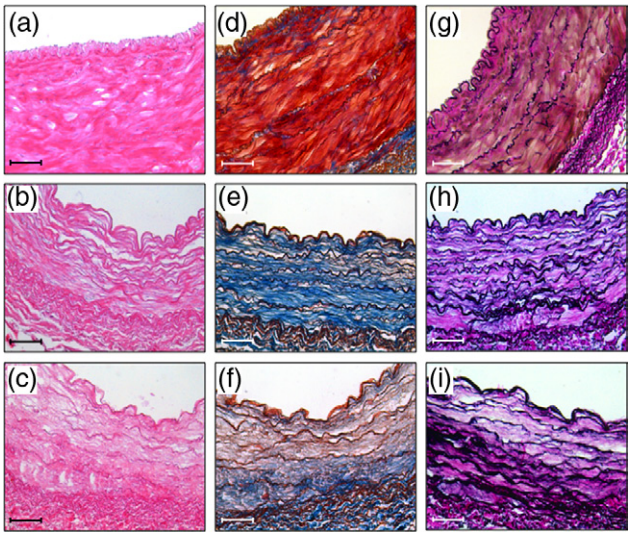

Figure 2. Histology. (*a–c*): (H&E) staining of native carotid (*a*) and decellularized arteries after SDS (*b*) and Trypsin and Triton X-100 (*c*) treatments. In (*a*) cell nuclei are stained blue-purple, extracellular fibers and cytoplasm are stained pink. In (*b*) and (*c*) complete removal of nucleic components is evident. (*d–f*): Masson's trichrome staining of native carotid (*d*) and decellularized arteries after SDS (*e*) and Trypsin and Triton X-100 (*f*) treatments. In (*d*) collagen fibers are shown in blue, muscle cells in red, elastic fibers in brown, and nuclei in black-brown. No residual red staining is present in (*e*) and (*f*), thus confirming cell removal, whereas the fibrillary component is preserved in both samples, as confirmed by deep blue collagen and light brown elastic fibers. (*g–i*): Verhoeff-van Gieson trichrome staining of native carotid (*g*) and decellularized arteries after SDS (*h*) and Trypsin and Triton X-100 (*i*) treatments. In (*g*) elastic fibers are shown in black, collagen in pink-purple, and cytoplasm in brown. In (*h*) and (*i*) elastic and collagen fibers are well-preserved, but cytoplasmic brown staining is completely lost. Scale bars indicate 100 μm.

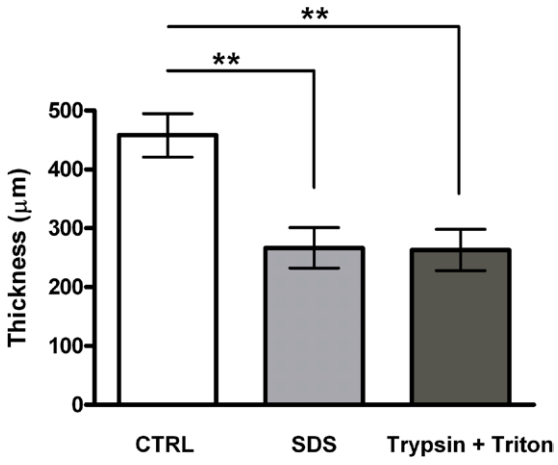

Figure 3. Vessel thickness measurement. Morphometric analysis demonstrates a significant reduction in carotid thickness after both SDS (n = 8) and Trypsin and Triton X-100 (n = 8) treatments compared to native arteries (n = 6). Data represent mean ± standard deviation. ** $p < 0.001$ after one-way ANOVA test. CTRL: control samples.

$\sigma_c = (1/2s) \times (p(t) \times De(t))$. The equivalent pressure can then be obtained by comparing the two previous equations as:

$$p(t) = F(t) / (D_e(t) \times L_n).$$

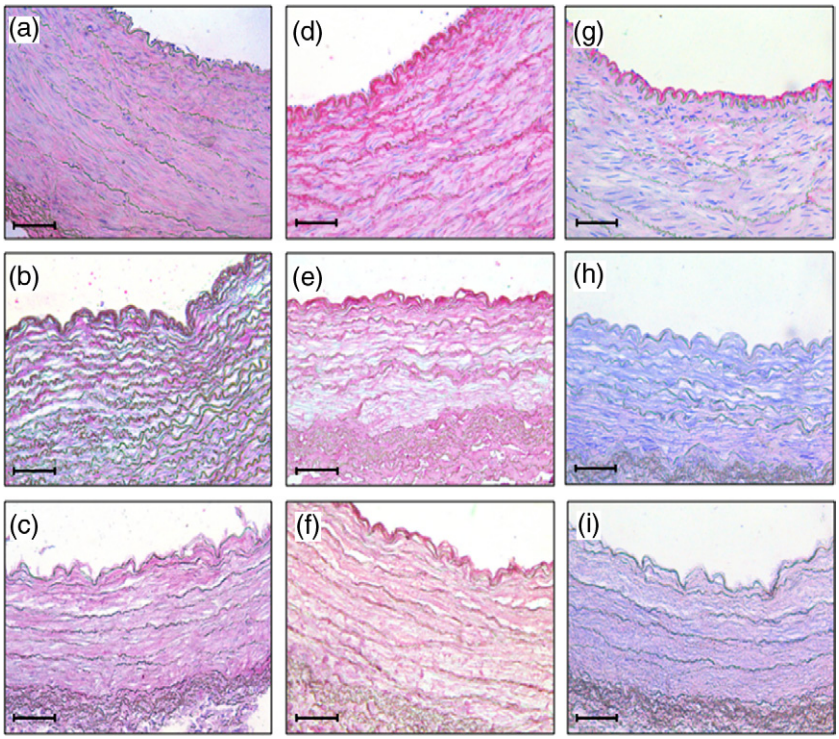

Figure 4. Immunohistochemistry. (*a–c*): Collagen type I distribution in native carotid (*a*) and decellularized arteries after SDS (*b*) and Trypsin and Triton X-100 (*c*) treatments. Specific immunolabeling is evident throughout the wall thickness in all samples. (*d–f*): Fibronectin expression is confined in the tunica intima in native carotid (*d*) and decellularized arteries after SDS (*e*) and Trypsin and Triton X-100 (*f*) treatments. (*g–i*): Laminin localization in native carotid (*g*) and decellularized arteries after SDS (*h*) and Trypsin and Triton X-100 (*i*) treatments. In (*g*) laminin is abundant in the basal membrane, while it cannot be identified in (*h*) and (*i*). Specific labeling is always shown in pink–red. Scale bars indicate 100 μm.

Finally, the compliance is given by:

$$C = ((D^2_{e\,max} - D^2_{e\,min})/D^2_{e\,min}) \times 1/\Delta P_e,$$

where ΔP_e represents the difference between maximum and minimum pressure applied during the sinusoidal cycle.

Details of the analysis for the compliance evaluation are reported elsewhere [35].

2.11. Statistical analysis

Results are expressed as the mean ± standard deviation related to at least three different vessels. Statistical differences were determined performing a one-way ANOVA test. A p value of < 0.05 was considered statistically significant.

3. Results

3.1. Histological and morphometric analysis

Histological sections of native and decellularized carotids are reported in figure 2. (H&E) staining clearly shows complete removal of cellular and nucleic components in the vessels treated with the two proposed protocols when considering both the luminal surface and the underlying matrix scaffolding. Masson's trichrome and Verhoeff-van Gieson stainings provide evidence of well preserved collagen and elastic fibers, respectively. More important, images demonstrate the preservation of the inner and outer elastic laminae after decellularization occurs.

As a consequence of the removal of muscle cells from the tunica media shown by means of histological stainings, wall thickness undergoes a significant reduction ($p < 0.001$) after both decellularization protocols as it may be seen from figure 3. Specifically, the reduction level is equal to 41.8% ± 7.5% for SDS and 42.6% ± 7.6% for Trypsin and Triton X-100 treated vessels, respectively, as compared to native carotids.

3.2. Immunohistochemistry

As is apparent from figure 4, immunolocalization of collagen type I reveals faint but uniform labeling throughout the wall thickness in both native and decellularized arteries. It should be noted that basal membrane proteins, fibronectin and laminin are evident underneath the endothelial layer in control samples. While fibronectin is preserved in decellularized vessels, laminin immunoreactivity is totally lost after both treatments, as it may be seen from figure 4.

3.3. Scanning electron microscopy

SEM examination focused primarily on the luminal surface of the carotids. As shown in figure 5, an intact layer of endothelial cells is present in the native artery. On the other hand, cells have been completely eliminated after the decellularization

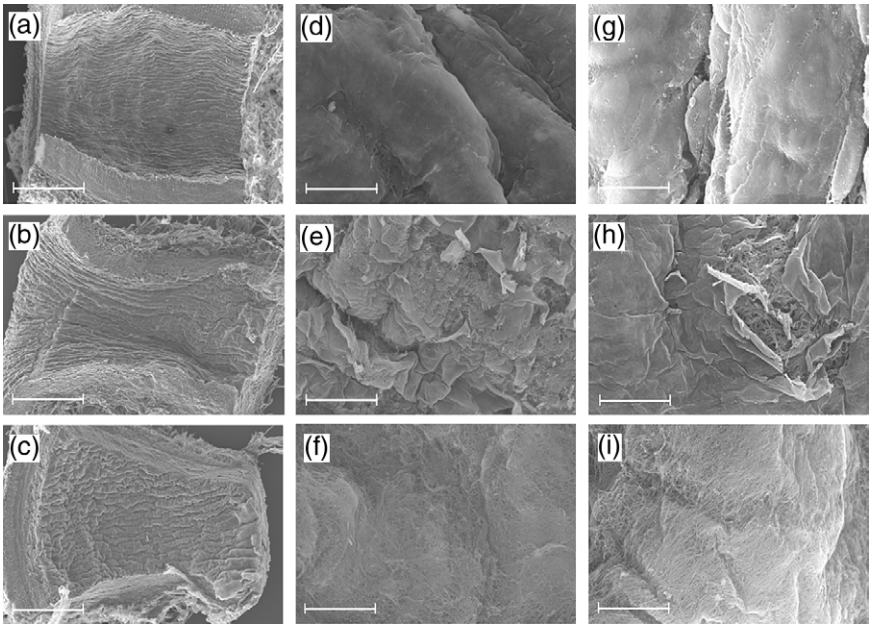

Figure 5. Scanning electron microscopy. Ultrastructure of native (*a*, *d*, *g*) and decellularized carotids after SDS (*b*, *e*, *h*) and Trypsin and Triton X-100 (*c*, *f*, *i*) treatments. Lower magnification photomicrographs show well-preserved morphology in all samples (*a–c*). At higher magnification, luminal surface appears to be covered by an intact and smooth endothelial monolayer in native carotids (*d* and *g*). After SDS treatment, the protein network typical of the basal membrane is visible together with few endothelial membrane residues (*e* and *h*). No cell debris is present in the luminal surface of Trypsin and Triton X-100 treated carotids (*f* and *i*), thus confirming complete removal of endothelium. Scale bars indicate 600 μm (*a–c*), 16.7 μm (*d–f*), and 10 μm (*g–i*).

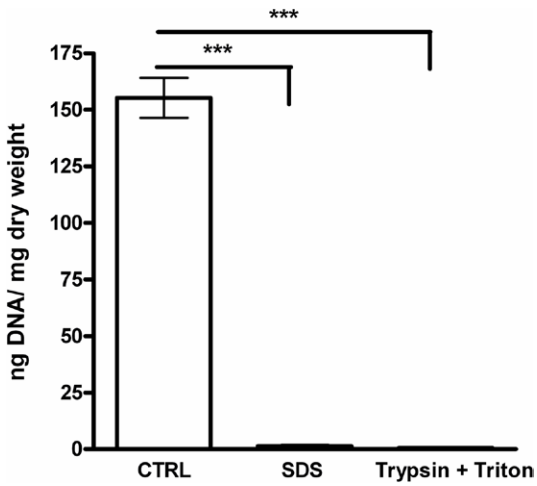

Figure 6. DNA quantification. DNA content for native and decellularized ovine carotids (n = 3 for each experimental group) expressed as ng per mg of dried tissue; data represent mean ± standard deviations. *** $p < 0.0001$ after one-way ANOVA test.

and a network of fibers is revealed figure 5. From figure 5 it may be seen that under higher magnification detailed porous structures may be revealed. The latter ones appeared to be distinct holes, previously occupied by cells.

3.4. DNA quantification

The analysis of DNA content, performed as described in section 2.7, confirms the effective carotid decellularization. As shown in figure 6, DNA content of native blood vessels is 155.3 ± 8.8 ng per mg tissue dry weight, whereas acellular carotids contain1.37 ± 0.51 ng mg^{-1} in SDS treated samples, and 0.69 ± 0.06 ng mg^{-1} in Trypsin and Triton X-100 treated ones, respectively. Data indicate that there is a significant reduction ($p < 0.0001$) in DNA levels following both decellularization protocols.

3.5. Influence of conditioned media on human mesenchymal stem cell growth

Conditioned media, prepared as described in section 2.8 by washing decellularized vessel segments in hMSCs growth medium for four days, were assessed to demonstrate their capability to promote hMSC proliferation in comparison to standard growth medium. As shown in figure 7(*a*), none of the conditioned media negatively affect cell growth as compared to the untreated culture medium.

3.6. Cell seeding onto decellularized carotids

To assess the suitability of the decellularized blood vessels to sustain hMSC adhesion and survival on the luminal surface, qualitative analysis of hMSC adhesion after 96 hours of static culture was performed. Figures 7(*b* and *c*) reveal adhesion of cells on both SDS and Trypsin and Triton X-100 treated arteries, moreover cells show their physiological morphology after adhesion on both samples.

3.7. Mechanical testing

The stress-strain curves representative of the mechanical behavior of decellularized and native carotids are shown in figure 8(*a*). SDS treated vessels exhibit a higher Young's modulus, both in longitudinal and circumferential direction,

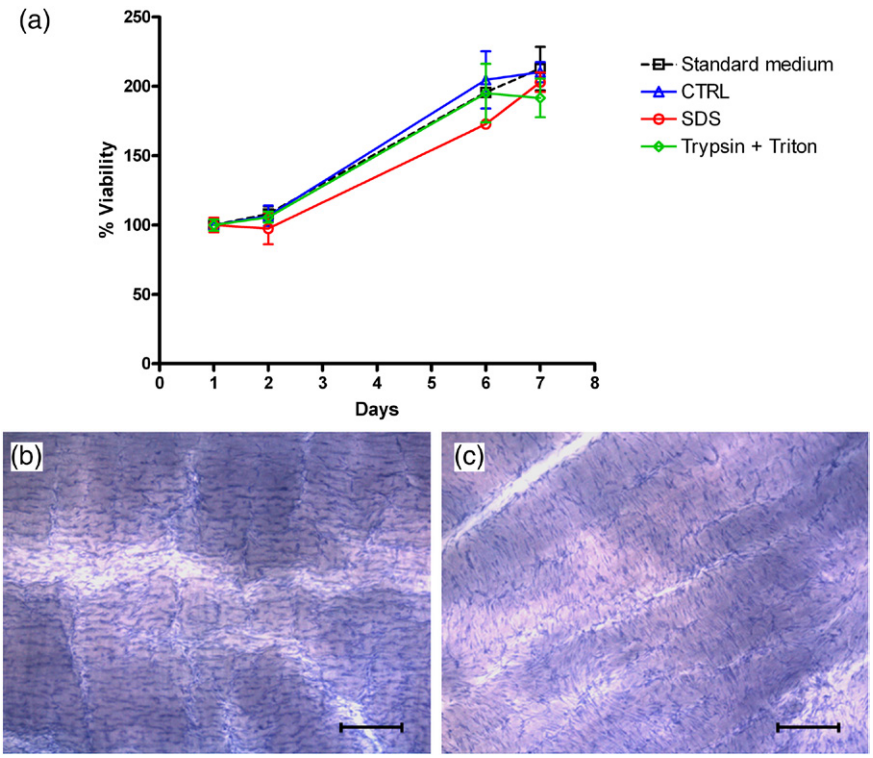

Figure 7. Biocompatibility assays. (*a*): Effect of conditioned media on hMSCs proliferation. The percentage of viability is shown after 1, 2, 6, and 7 days of hMSCs incubation using conditioned media. None of them negatively affected cell growth as compared to the untreated culture medium. Data represent mean ± standard deviation (n = 3 for each experimental group). (*b*), (*c*): Representative image of cells (blue) seeded on the luminal surface of carotids decellularized with SDS (*b*) and Trypsin and Triton X-100 (*c*), respectively. Scale bars indicate 20 μm.

as compared to native carotids. On the other hand, the stress-strain curve representative of the Young's modulus for the vessels treated with Trypsin and Triton X-100 is similar to the one of native carotids. When considering the compliance, it may be seen from figure 8(*b*) that no significant difference ($p > 0.05$) is obtained between native carotids ($0.018083 \pm 0.001564\,mmHg^{-1}$) and those decellularized with Trypsin and Triton X-100 ($0.018917 \pm 0.006775\,mmHg^{-1}$), whereas SDS treated vessels show a significant ($p < 0.001$) lower mean value ($0.00533 \pm 0.000492\,mmHg^{-1}$).

4. Discussion and concluding remarks

Our results show that both proposed treatments induce effective cell removal in the whole vessels. This is confirmed by the absence of visible cells within the decellularized carotids following H&E staining in figure 2, SEM analysis in figure 5, and a significant reduction in DNA content in figure 6, thus satisfying the minimal criteria for decellularization [21]. Furthermore, histology by Masson's and Verhoeff-van Gieson's trichrome figure 2 demonstrate that vessels subjected to the proposed decellularization treatments are able to maintain their native structure without significant loss of total collagen and elastic fibers, thus suggesting no severe damage to the ECM structure. In addition, histological images confirm the preservation of inner and outer elastic laminae which are recognized as very important structures for endothelial cell attachment and resistance to thrombus formation [7]. This finding is also proved by SEM analysis in figure 5, where a well preserved protein network on the luminal surface of the decellularized carotids can be clearly seen.

Protocol efficiency is also confirmed by the significant decrease of the vessel thickness caused by both decellularization protocols in figure 3. Indeed, it is reasonable to assume that this variation is due to the removal of smooth muscle cell layer.

Immunohistochemical stainings in figure 4 reveal no significant evidence of alteration in collagen type I and fibronectin distribution when considering carotids decellularized with both protocols as compared to native ones. On the other hand, a total loss of laminin when taking advantage of both treatments is identified. It is worth noting that the presence of laminin, as well as of fibronectin, is fundamental for cell attachment and laminin is also involved in the migration and growth of endothelial cells [36, 37]. Therefore it has been necessary to verify the ability of the decellularized carotids to support cellular adhesion and proliferation. Referring to Cebotari [38], where it is demonstrated that a restricted number of washing cycles after decellularization induces a cytotoxic effect on endothelial cells, we first verified the removal of decellularizing agent traces in figure 7(*a*). Subsequently, we seeded hMSCs onto the luminal surface of the vessels, thus showing that, despite the loss of laminin, both the vessels allow hMSC attachment and growth in figure 7(*b*) and figure 7(*c*). Our results are in agreement with a previous work by Cortiella [39], where the repopulation of acellular lungs, even though laminin was no more detectable after decellularization, has been described.

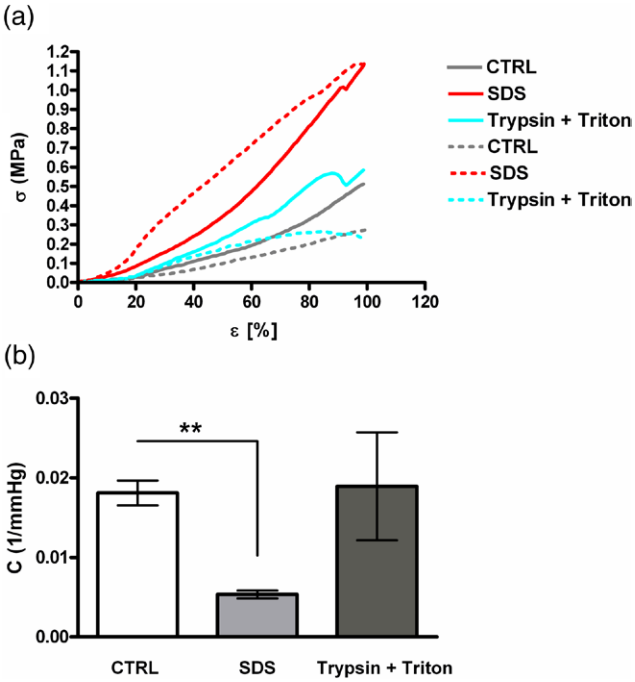

Figure 8. Mechanical testing. (*a*): Stress-strain curves of native and decellularized carotids (n = 3 for each experimental group). SDS treated vessels (red lines) show a higher Young's modulus, both in longitudinal (solid lines) and circumferential (dotted lines) directions, as compared to controls (gray lines), whereas Trypsin and Triton X-100 treated arteries (blue lines) are similar to native ones. (*b*): Compliance analysis (n = 3 for each experimental group) demonstrates a significant difference between data from native carotids and those one related to SDS treated vessels. No statistically significant discrepancy is found between control samples and those decellularized with Trypsin and Triton X-100. Data represent mean ± standard deviation. ** $p < 0.001$ after one-way ANOVA test. CTRL: control samples.

Thus it is reasonable to think that its loss does not prevent the repopulation of the scaffolds decellularized in this work.

With respect to mechanical characterization of vessels, Young's modulus and compliance show no significant differences between carotids decellularized with Trypsin and Triton and native ones in figure 8. On the other hand, SDS treated samples show a higher elastic modulus in both longitudinal and circumferential direction, and a lower value of compliance. It should be noted that a higher elastic modulus and a lower compliance are closely related to the increase of vascular stiffness. Similar results are obtained by Roy *et al* [40], who analyze the biomechanical properties of SDS decellularized porcine carotids. Specifically, a higher elastic modulus and a lower compliance in the decellularized samples compared to native arteries were found.

The ideal vascular graft should be biocompatible and resistant to thrombosis and infection, but it should also be elastic and match the compliance with the native host vessel [10]. Different mechanical behavior between the graft and the native vessel could in fact induce local flow disturbance and facilitate thrombus formation. Indeed, it has been shown in previous studies that endothelial hyperplasia could be related to compliance mismatch at the anastomosis [41–43]. Bearing in mind our results, SDS, Trypsin and Triton treatments have proved to be effective in removing the cellular and nucleic material from sheep carotid, maintaining apparently unchanged ECM features. Actually, the treatment with SDS determines important alterations at the level of mechanical properties of the vessel. Therefore, in our opinion, the combination of a non-ionic detergent (Triton X-100) with an enzymatic treatment (Trypsin), at the concentrations used in this study, is more effective than ionic treatment (SDS) with the aim of producing an acellular small artery, from ovine carotid, suitable for vascular graft achievement.

Acknowledgements

The financial support of project PRODERIVASA granted by Sardegna Ricerche, Italy is gratefully acknowledged. One of us (L. Mancuso) has performed her activity in the framework of the PhD in Biomedical Engineering at the University of Cagliari, Italy.

Disclosure

The authors declare no conflict of interests.

References

[1] Rosamond W *et al* 2008 Heart disease and stroke statistics - 2008 update - A report from the American Heart Association Statistics Committee and Stroke Statistics Subcommittee *Circulation* **117** E25–E146
[2] Kannan R Y, Salacinski H J, Butler P E, Hamilton G and Seifalian A M 2005 Current status of prosthetic bypass grafts: A review *J. Biomed. Mat. Res. Part B-Appl. Biomaterials* **74** 570–81
[3] Klinkert P, Post P N, Breslau P J and van Bocke J H 2004 Saphenous vein versus PTFE for above-knee femoropopliteal bypass. a review of the literature. *Eur. J. Vasc. Endovasc. Surg.* **27** 357–62
[4] Chard R B, Johnson D C, Nunn G R and Cartmill T B 1987 Aorta-coronary bypass grafting with polytetrafluoroethylene conduits early and late outcome in eight patients *J. Thorac. Cardiovasc. Surg.* **94** 132–34
[5] Canver C C 1995 Conduit options in coronary-artery bypass-surgery *Chest* **108** 1150–5
[6] Seifu D G, Purnama A, Mequanint K and Mantovani D 2013 Small-diameter vascular tissue engineering *Nat .Rev. Cardiol.* **10** 410–21
[7] Wilshaw S P *et al* 2012 Development and characterization of acellular allogeneic arterial matrices *Tissue Eng. Part A* **18** 471–83
[8] Badylak S F, Freytes D O and Gilbert T W 2009 Extracellular matrix as a biological scaffold material: Structure and function *Acta Biomater.* **5** 1–13
[9] Ketchedjian A *et al* 2005 Ovine panel reactive antibody assay of HLA responsivity to allograft bioengineered vascular scaffolds *J. Thorac. Cardiovasc. Surg.* **129** 159–66
[10] Bergmeister H, Strobl M, Grasl C, Liska R and Schima H 2013 Tissue engineering of vascular grafts *Eur. Surg.* **45** 187–3
[11] Rosellini E, Vozzi G, Barbani N, Giusti P and Cristallini C 2010 Three-dimensional microfabricated scaffolds with cardiac extracellular matrix-like architecture *Int. J. Artif. Organs* **33** 885–94

[12] Quint C, Kondo Y, Manson R J, Lawson J H, Dardik A and Niklason L E 2011 Decellularized tissue-engineered blood vessel as an arterial conduit *Proc. Natl. Acad. Sci. USA* **108** 9214–9

[13] Birchall M and Hamilton G 2012 Tissue-engineered vascular replacements for children *Lancet* **380** 197–8

[14] Olausson M *et al* 2012 Transplantation of an allogeneic vein bioengineered with autologous stem cells: a proof-of-concept study *Lancet* **380** 230–7

[15] Quint C, Arief M, Muto A, Dardik A and Niklason L E 2012 Allogeneic human tissue-engineered blood vessel *J. Vasc. Surg.* **55** 790–8

[16] D'Onofrio A *et al* 2011 Clinical and Hemodynamic Outcomes after Aortic Valve Replacement with Stented and Stentless Pericardial Xenografts: A Propensity-Matched Analysis *J. Heart. Valve. Dis.* **20** 319–26

[17] Macchiarini P *et al* 2008 Clinical transplantation of a tissue-engineered airway *Lancet* **372** 2023–30

[18] Ricchetti E T, Aurora A, Iannotti J P and Derwin K A 2012 Scaffold devices for rotator cuff repair 2012 *J. Shoulder Elbow Surg.* **21** 251–65

[19] Martinello T *et al* 2012 Successful recellularization of human tendon scaffolds using adipose-derived mesenchymal stem cells and collagen gel *J. Tissue Eng. Regen. Med.* doi:10.1002/term.1557

[20] Meyer T, Schwarz K, Ulrichs K and Hocht B 2006 A new biocompatible material (Lyoplant (R)) for the therapy of congenital abdominal wall defects: first experimental results in rats *Pediatr. Surg Int.* **22** 369–74

[21] Crapo P M, Gilbert T W and Badylak S F 2011 An overview of tissue and whole organ decellularization processes *Biomaterials* **32** 3233–43

[22] Catto V, Farè S, Freddi G and Tanzi M C 2014 Vascular Tissue Engineering: Recent Advances in Small Diameter Blood Vessel Regeneration *ISRN Vascular Med.* doi:10.1155/2014/923030

[23] Ott H C *et al* 2008 Perfusion-decellularized matrix: using nature's platform to engineer a bioartificial heart *Nature Med.* **14** 213–21

[24] Petersen T H *et al* 2010 Tissue-Engineered Lungs for in Vivo Implantation *Science* **329** 538–41

[25] Bao J *et al* 2011 Construction of a Portal Implantable Functional Tissue-Engineered Liver Using Perfusion-Decellularized Matrix and Hepatocytes in Rats *Cell Transpl.* **20** 753–66

[26] Song J J *et al* 2011 Enhanced In Vivo Function of Bioartificial Lungs in Rats *Ann. Thorac. Surg.* **92** 998–6

[27] Sullivan D C *et al* 2012 Decellularization methods of porcine kidneys for whole organ engineering using a high-throughput system *Biomaterials* **33** 7756–64

[28] Gilbert T W, Sellaro T L and Badylak S F 2006 Decellularization of tissues and organs *Biomaterials* **27** 3675–83

[29] Böer U, Lohrenz A, Klingenberg M, Pich A, Haverich A and Wilhelmi M 2011 The effect of detergent-based decellularization procedures on cellular proteins and immunogenicity in equine carotid artery grafts *Biomaterials* **32** 9730–7

[30] Dahan N, Zarbiv G, Sarig U, Karram T, Hoffman A and Machluf M 2012 Porcine small diameter arterial extracellular matrix supports endothelium formation and media remodeling forming a promising vascular engineered biograft *Tissue Eng. Part A* **18** 411–22

[31] Riva A, Faa G, Loffredo F, Piludu M and Testa Riva F 1999 An improved OsO4 maceration method for the visualization of Internal structures and surfaces in human bioptic specimens by high resolution scanning electron microscopy *Scanning Microscopy* **13** 111–22

[32] Riva A *et al* 2007 New findings on 3-D microanatomy of cellular structures in human tissues and organs. An HRSEM study *Eur. J. Histochem.* **51** 53–8

[33] Scanu M, Mancuso L and Cao G 2011 Evaluation of the use of human mesenchymal stem cells for acute toxicity tests *Toxicol in Vitro* **25** 1989–95

[34] Mangold S *et al* 2012 Evaluation of decellularized human umbilical vein (HUV) for vascular tissue engineering—comparison with endothelium-denuded HUV *J. Tissue Eng. Regen. Med.* doi:10.1002/term.1603

[35] Quaglini V *et al* 2002 An in vitro methodology for evaluating the mechanical properties of aortic vascular prostheses *Artif. Organs* **26** 555–64

[36] Kleinman H, McGarvey M, Hassel J, Martin G, Baron van Evercooren A and Dubois-Dalcq M 1984 *The role of extracellular matrix in development* ed R L Trelstad (New York: Liss) pp 123–43

[37] Timpl R and Brown J C 1994 The laminins *Matrix Biol.* **14** 275–81

[38] Cebotari S *et al* 2010 Detergent decellularization of heart valves for tissue engineering: toxicological effects of residual detergents on human endothelial cells *Artif. Organs* **34** 206–9

[39] Cortiella J *et al* 2010 Influence of acellular natural lung matrix on murine embryonic stem cell differentiation and tissue formation *Tissue Eng. Part A* **16** 2565–80

[40] Roy S, Silacci P and Stergiopulos N 2005 Biomechanical proprieties of decellularized porcine common carotid arteries *Am. J. Physiol. Heart. Circulatory. Physiol.* **289** H1567–76

[41] Okuhn S P, Connelly D P, Calakos N, Ferrell L, Pan M X and Goldstone J 1989 Does compliance mismatch alone cause neointimal hyperplasia? *J. Vasc. Surg.* **9** 35–45

[42] Ballyk P D, Walsh C, Butany J and Ojha M 1998 Compliance mismatch may promote graft-artery intimal hyperplasia by altering suture-line stress *J. Biomech.* **31** 229–37

[43] Greenwald S E and Berry C L 2000 Improving vascular grafts: the importance of mechanical and haemodynamic properties *J. Pathol.* **190** 292–99